Journal of the Mechanics and Physics of Solids 74 (2015) 68–79

Contents lists available at ScienceDirect

Journal of the Mechanics and Physics of Solids

journal homepage: www.elsevier.com/locate/jmps

Smoothening creases on surfaces of strain-stiffening materials

Lihua Jin, Zhigang Suo *

School of Engineering and Applied Sciences, Kavli Institute for Nanobio Science and Technology, Harvard University, Cambridge, MA 02138, USA

ARTICLE INFO

Article history:
Received 6 February 2014
Received in revised form
7 August 2014
Accepted 15 October 2014
Available online 23 October 2014

Keywords:
Mechanical instability
Crease
Strain-stiffening material
Gent material

ABSTRACT

When an elastic block (e.g., an elastomer or a soft tissue) is compressed to a critical strain, the smooth surface of the block forms creases, namely, localized regions of self-contact. Here we show how this instability behaves if the solid stiffens steeply. For a solid that stiffens steeply at large strains, as the compression increases, the surface is initially smooth, then forms creases, and finally becomes smooth again. For a solid that stiffens steeply at small strains, creases will never form and the surface remains smooth for all levels of compression. We also obtain the critical conditions for the onset of wrinkles. When the surface does become unstable, we find that creases always set in at a lower compression than wrinkles. Our findings may shed light in developing crease-resistant materials

1. Introduction

Biot (1963) analyzed an elastic block compressed under the plane strain conditions (Fig. 1a and b), and predicted that the flat surface of the block was unstable when the compression reached a critical strain of 0.46. This theoretical prediction remained unchallenged until Gent and Cho (1999) noted its disagreement with their experimental finding that the surface formed creases at a critical strain of 0.35. Hohlfeld (2008) and Hohlfeld and Mahadevan (2011) showed that Biot's solution and creases are two distinct instabilities, and that creases set in at a critical strain of 0.35. Biot linearized the boundary-value problem around a state of finite homogeneous deformation, and his solution corresponds to a smooth, wavy surface (i.e., wrinkles) of small strain relative to the homogeneous state (Fig. 1c). By contrast, a crease is a localized, self-contact region of large strain relative to the homogeneous state (Fig. 1d). The critical strain for the onset of creases has since been obtained by several other approaches of numerical analysis (Hong et al., 2009; Wong et al., 2010; Cai et al., 2010; Hong and Gao, 2013; Tallinen et al., 2013). Furthermore, Hohlfeld (2013) mapped the onset of a crease to the coexistence of two scale-invariant states. A post-bifurcation analysis of Cao and Hutchinson (2012) showed that Biot's solution is unstable.

No evidence exists that Biot's smoothly wavy surfaces have ever been observed experimentally on homogeneous elastic blocks under compression. Creases, however, have been observed routinely on elastic blocks compressed by various means, including mechanical forces (Cai et al., 2012; Gent and Cho, 1999; Ghatak and Das, 2007; Mora et al., 2011), constrained swelling (Arifuzzaman et al., 2012; Barros et al., 2012; Dervaux and Ben Amar, 2012; Dervaux et al., 2011; Guvendiren et al., 2010; Ortiz et al., 2010; Pandey and Holmes, 2013; Tanaka, 1986; Tanaka et al., 1987; Trujillo et al., 2008; Weiss et al., 2013; Zalachas et al., 2013), temperature change (Kim et al., 2010), electric fields (Park et al., 2013; Wang et al., 2012; Wang et al., 2011; Wang and Zhao, 2013a; Xu and Hayward, 2013), and light (Yoon et al., 2012). Creases have been studied in soft tissues

* Corresponding author.
E-mail address: suo@seas.harvard.edu (Z. Suo).

http://dx.doi.org/10.1016/j.jmps.2014.10.004
0022-5096/

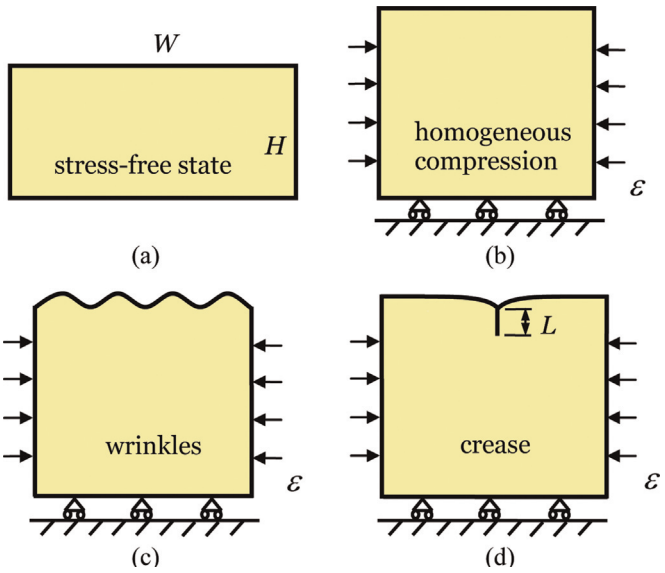

Fig. 1. (a) In the stress-free state, a block of elastic material is of width W and height H. Under compression the material may deform in several ways. (b) The block undergoes homogeneous compression. (c) The surface forms wrinkles. (d) The surface forms a crease of depth L. The applied strain ε is defined by the compressive displacement divided by the initial width of the block.

(Bayly et al., 2014; Jin et al., 2011; Yang et al., 2007). Creases have been related to the Schallamach waves arising during the frictional sliding of a rubber against a rigid surface (Gabriel et al., 2010), and to the osmotic collapse of a water-filled cavity in a hydrogel (Cai et al., 2010). Creases can also form on the interface between two elastic solids (Jin et al., 2014). Applications of creases have been explored, including the use of creases to control chemical patterns (Kim et al., 2010; Yoon et al., 2012), enzymatic activity (Kim et al., 2010), cellular behavior (Saha et al., 2010), adhesion (Chan et al., 2011), and biofouling (Shivapooja et al., 2013).

Although wrinkles have never been observed experimentally on large homogeneous elastic blocks under compression, many factors affect the behavior of creases, and may even promote the formation of wrinkles. Surface energy adds a barrier to the nucleation of creases, and makes nucleation defect-sensitive (Chen et al., 2012; Yoon et al., 2010). When the loading is an electric field, wrinkles may form when the elastocapillary effect is strong enough (Wang and Zhao, 2013a). For a layer of finite thickness with a traction-free bottom surface, creases on the top surface are subcritical—that is, as the applied compressive strain increases and then decreases, creases form and disappear with hysteresis (Hohlfeld and Mahadevan, 2012). For a stiff film on a soft substrate under compression, the film forms periodic wrinkles at a small strain (Bowden et al., 1998). As the strain increases, the wrinkles double their period, and ultimately lead to deep folds (Pocivavsek et al., 2008). When the film and the substrate have comparable moduli, the transitions between creases, wrinkles and folds become complex (Hutchinson, 2013; Wang and Zhao, 2013b). Complex behavior also occurs in a solid of gradient modulus (Diab et al., 2013; Wu et al., 2013). If the substrate is pre-compressed, creases are subcritical, and form and disappear with hysteresis (Chen et al., 2014).

Biot's original analysis, as well as much of the subsequent theoretical work, represents the elastic solid by the neo-Hookean model. This model describes elastomers of long polymer chains well, but is inadequate when materials stiffen steeply. A soft biological tissue, for example, is usually a composite of a compliant matrix and stiff fibers (Fung, 1993). When the tissue is under a small strain, the matrix carries much of the load, but the fibers are not tight, so that the tissue is soft. As the strain increases, the fibers gradually tighten and rotate to the loading direction, so that the tissue stiffens steeply. As another example, an elastomer is a three-dimensional network of long and flexible polymer chains (Treloar, 1975). When the elastomer is under no stress, the chains undergo thermal motion and coil. When the elastomer is subject to moderate strains, the chains uncoil and the stress–strain relation of the elastomer is well represented by the neo-Hookean model, which is derived under the assumption of Gaussian chains. When the chains become nearly straight, however, they no longer obey the Gaussian statistics, and the stress–strain curve rises steeply and deviates significantly from the neo-Hookean model. Destrade et al. (2009) analyzed the onset of wrinkles on the surface of a bending block. They showed that when the material stiffens at a relatively small strain, the critical strain for the onset of wrinkles differs significantly from that of a neo-Hookean material. These authors, however, did not consider the formation of creases.

Here we represent a strain-stiffening material by using the Gent model (Gent, 1996), and study the initiation and development of creases by using a finite element method. For a solid that stiffens at large strains, as the compression increases, the surface is initially smooth, then forms creases, and finally becomes smooth again. For a solid that stiffens at small strains, creases will never form and the surface remains smooth for all levels of compression. We also study the condition for the

onset of wrinkles by using linear perturbation. If a strain-stiffening material does become unstable under compression, we find that creases—rather than wrinkles—will form.

2. Strain-stiffening materials

We list the equations that govern the boundary-value problems of finite elasticity (Holzapfel, 2000). A body deforms in space from the stress-free state to a current state. In the body, a material particle is at spatial location $\mathbf{X}$ in the stress-free state, and is at spatial location $\mathbf{x}$ in the current state. The function $\mathbf{x}(\mathbf{X})$ describes the deformation of the body from the stress–free state to the current state. The deformation gradient is

$$F_{iK} = \frac{\partial x_i(\mathbf{X})}{\partial X_K}. \tag{1}$$

Let s_{iK} be the nominal stress. The balance of forces requires that

$$\frac{\partial s_{iK}}{\partial X_K} = 0. \tag{2}$$

The balance of forces also requires that

$$s_{iK} N_K = T_i, \tag{3}$$

where N_K is the unit vector normal to a small flat region in the body in the stress-free state, and T_i is the nominal traction (i.e., the force applied on the region in the current state divided by the area of the region in the stress-free state).

The body is made of an elastic material, taken to be incompressible

$$det(\mathbf{F}) = 1 \tag{4}$$

The density of the Helmholtz free energy is a function of the deformation gradient, $\psi(\mathbf{F})$. The equation of state is

$$s_{iK} = \frac{\partial \psi(\mathbf{F})}{\partial F_{iK}} - \Pi H_{iK}, \tag{5}$$

where $\mathbf{H} = \mathbf{F}^{-T}$, and Π is a hydrostatic pressure to be determined by the boundary-value problem. When the material undergoes a rigid-body rotation, the free energy is invariant, so that ψ depends on $\mathbf{F}$ through the Green deformation tensor $\mathbf{F}^T\mathbf{F}$. This dependence, together with (5), implies the balance of moments acting on any small part of the body, $s_{iK}F_{jK} = s_{jK}F_{iK}$.

Following Gent (1996), we model strain-stiffening materials by using the free energy function

$$\psi = -\frac{\mu}{2} J_{lim} log\left(1 - \frac{J_1}{J_{lim}}\right). \tag{6}$$

The Gent model represents the magnitude of deformation by a single scalar, $J_1 = F_{iK}F_{iK} - 3$. The model has two material parameters, μ and J_{lim}. In the limit of small deformation, $J_1/J_{lim} \to 0$, the Gent model recovers the neo-Hookean model $\psi = \mu J_1/2$, with μ being the shear modulus. In the limit of large deformation, $J_1/J_{lim} \to 1$, the free energy diverges and the stress–strain curve turns vertical. The parameter J_{lim} represents the limiting deformation. The stress–strain relation of the Gent materials is

$$s_{iK} = \frac{\mu}{1 - J_1/J_{lim}} F_{iK} - \Pi H_{iK}. \tag{7}$$

For a block in a state of homogeneous, plane-strain deformation, when the width changes by a factor of λ, the height changes by a factor of λ^{-1}, and the deformation gradient is

$$\mathbf{F} = \begin{bmatrix} \lambda & 0 & 0 \\ 0 & 1 & 0 \\ 0 & 0 & \lambda^{-1} \end{bmatrix}. \tag{8}$$

The nominal stress in the direction of compression is

$$s = \frac{\mu(\lambda - \lambda^{-3})}{1 - (\lambda^2 + \lambda^{-2} - 2)/J_{lim}}. \tag{9}$$

In obtaining (9), we have used the traction-free boundary condition $s_{33} = 0$, which gives $\Pi = \mu\lambda^{-2}/\left(1 - (\lambda^2 + \lambda^{-2} - 2)/J_{lim}\right)$. Define the compressive strain by $\varepsilon = 1 - \lambda$. For a given value of J_{lim}, the stress–strain curve turns vertical at a limiting strain ε_{lim} (Fig. 2a). The limiting strain increases with J_{lim} (Fig. 2b).

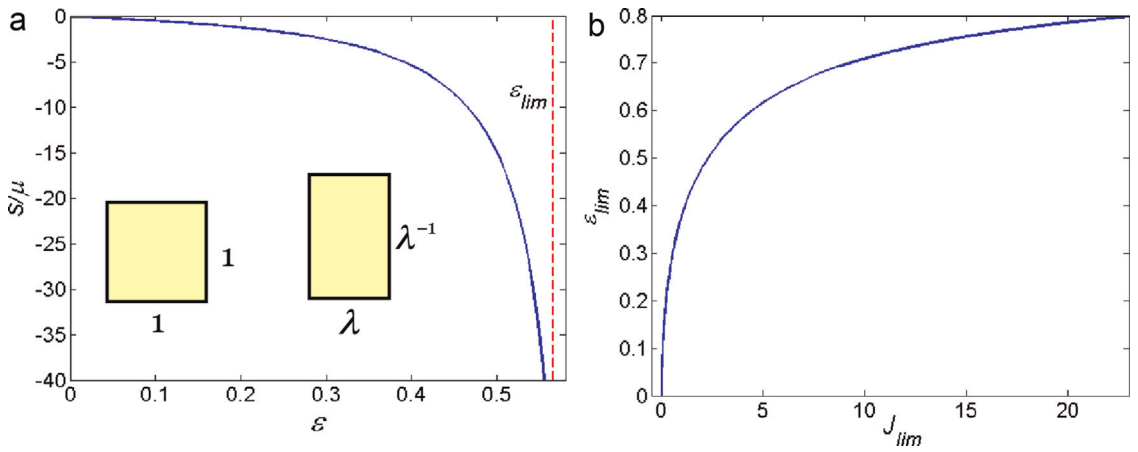

Fig. 2. The Gent model characterizes a strain-stiffening material with two parameters: μ and J_{lim}. (a) The compressive stress–strain curve for a Gent material with $J_{lim} = 4.5$. A unit cube is compressed under the plane strain condition, with the width changing by a factor of λ, the height changing by a factor of λ^{-1}. The compressive strain is defined by $\varepsilon = 1 - \lambda$, and the stress s is normalized by μ. The stress–strain curve turns vertical at the limiting strain $\varepsilon_{\lim}$. (b) The limiting strain $\varepsilon_{\lim}$ increases with J_{lim}.

3. Creases

We study the initiation and development of creases by using the finite element software ABAQUS. We implement the Gent model by writing a user-defined subroutine UMAT (Appendix B), which is available online as the Supplementary information of this paper. We assume that surface of the solid forms a periodic array of creases, and one period of the solid is a block of width W and height H in the stress-free state (Fig. 1a). The width W of the block is assumed to be 3.5 times of the height H of the block, a ratio that is representative of experimental observations (Cai et al., 2012). Taking advantage of the symmetry of a crease, we only simulate one half of the block. We fix the horizontal position of the mid-plane of the block, compress the block under the plane strain conditions by prescribing horizontal displacement on the edge of the block, and fix the vertical position of the bottom plane of the block (Fig. 1d). To break the translational symmetry, we place a quarter of a small circle on the surface as a defect. The size of the defect is much smaller than the length scale of the problem, H. In the vicinity of the defect, we resolve the field by using meshes much smaller than the size of the defect.

Our calculation shows that, as the applied compressive strain increases, the surface is initially flat, then forms a crease, and finally becomes flat again. This surprising sequence of development is understood by inspecting the distribution of deformation in the block at several values of the applied compressive strain (Fig. 3). Here the particular sequence is calculated using a Gent material with $J_{\lim} = 4.5$. The colors correspond to the values of the scalar measure of deformation, J_1. Recall that the free energy density ψ is a monotonic function of J_1. At $\varepsilon = 0.351$, the surface of the block is flat and the deformation in the block is homogeneous (Fig. 3a). A crease initiates at the critical strain $\varepsilon = 0.396$. After the crease sets in, the deformation becomes inhomogeneous. The formation of the crease reduces deformation in a T-shaped region close to the surface and in the region underneath the tip of the crease (Fig. 3b). However, in a wing-shaped region on the two sides near the tip of the crease (in green), the deformation exceeds the applied deformation. The two effects—the reduced deformation in the T-shaped region and the increased deformation in the wing-shaped region—compete. The combination of these two effects guarantees that the total energy of the creased state is lower than the flat state. Self-contact of the surface starts to form when the crease initiates, and the crease first grows deeper as the applied strain ε increases. However, the wing-shaped region also grows larger (Fig. 3c). Due to the strain-stiffening effect, the energy penalty in the wing-shaped region may increase faster than the energy reduction in the T-shaped region. When $\varepsilon = 0.498$, the crease depth is maximal (Fig. 3c). With the further increase of ε, the penalty of forming a deep crease is so high that the crease starts to smoothen instead. When $\varepsilon = 0.556$, both the crease depth and penalty region become smaller (Fig. 3d). When $\varepsilon = 0.579$, the surface becomes nearly flat again, and the value of J_1 in the whole block of material is close to $J_{\lim}$ (Fig. 3e). Interestingly, similar smoothening and disappearance of ridge instability was also predicted in strain-stiffening Arruda-Boyce materials with a small stretch limit (Zang et al., 2012).

We plot the bifurcation diagram by using the applied strain ε as the control variable, and the normalized crease depth L/H as a proxy for the state of the block (Fig. 4). For a Gent material of $J_{\lim} = 4.5$, the crease depth first grows larger as the strain ε increases. The crease depth reaches the maximal at the strain of $\varepsilon = 0.498$. With further increase of the strain ε, the crease depth starts to decrease, and the crease is smoothened. At strain $\varepsilon = 0.579$, the crease depth becomes zero again, and the crease disappears. The dependence of the normalized crease depth L/H on strain ε for other $J_{\lim}$ is also plotted in Fig. 4. For large values of J_{lim}, the limiting stretches are large, so that the mesh near the tip of the crease distorts severely when the compression goes close to the stretch limit. The computation remains stable to a larger applied strain as we refine the mesh further, but the computation will be extremely expensive to reach the disappearance of the creases. Therefore, we only included the results that show the clear growth and smoothening of creases. When $J_{\lim} \to \infty$, the material recovers the neo-

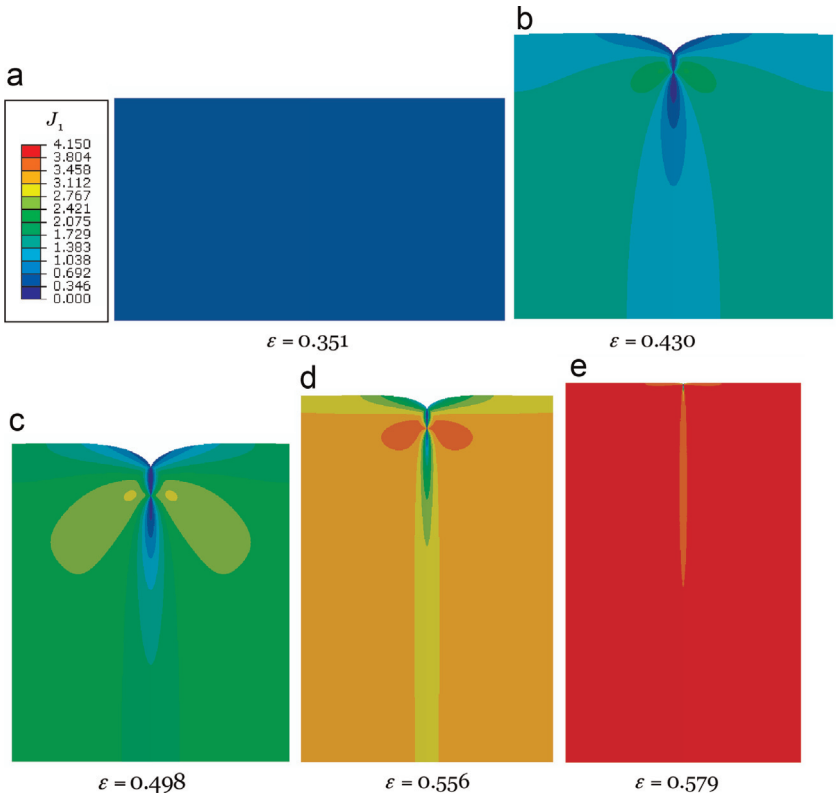

Fig. 3. As the applied strain ε increases, the surface is initially flat, then forms a crease, and finally becomes flat again. The calculation is carried out with a Gent material of $J_{lim} = 4.5$. (a)–(e) correspond to states at increasing levels of applied strain. The colors represent the scalar measure of the deformation, J_1. (For interpretation of the references to color in this figure legend, the reader is referred to the web version of this article.)

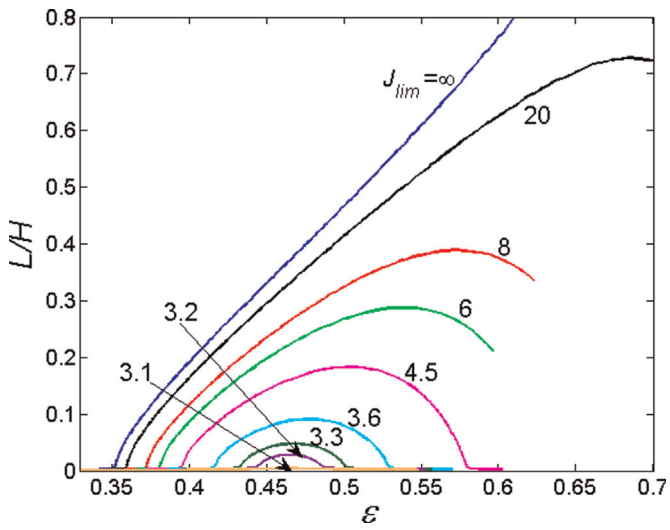

Fig. 4. The normalized crease depth L/H as a function of the applied strain ε. When $J_{\text{lim}} \to \infty$, the Gent model recovers the neo-Hookean model, and the crease initiates when ε reaches around 0.354. With the decrease of J_{lim}, the critical strain for the onset of the crease increases, and the crease disappears when the applied strain is large enough. When J_{lim} is below about 3.1, no crease forms at any strain.

Hookean material. The crease depth L/H is zero until a crease sets in at strain around 0.354. Then the crease depth L/H monotonically increases with ε. For finite J_{lim}, the creases always smoothen at some finite strain. With the decrease of J_{lim}, the critical strain for the onset of creases increases. At the same time, the strain for the disappearance of crease decreases with the decrease of J_{lim}. When $J_{\text{lim}} \leq 3.1$, creases are completely suppressed.

The conditions for the onset and disappearance of creases depend on the value of J_{lim} (Fig. 5). The lower part of the curve corresponds to the strain for the initiation of the crease, and the upper part of the curve corresponds to the strain for the

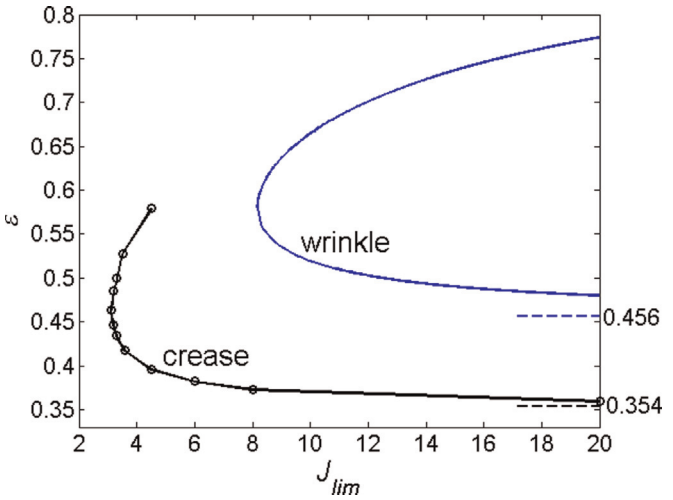

Fig. 5. The critical strains for the initiation and disappearance of a crease as a function of J_{lim}. The circles represent the results of finite element simulations. Also plotted are the critical conditions for the formation of wrinkles predicted by a linear perturbation analysis.

disappearance of the crease. No crease forms when $J_{\text{lim}} \leq 3.1$. Creases can only form in the region enclosed by the curve. The window of strain for the existence of creases decreases with the decreases of J_{lim}.

4. Wrinkles

When a body of a Gent material is compressed, will the flat surface of the body form wrinkles instead of creases? To answer this question, we determine the critical condition for the onset of wrinkles, and compare the condition with that for the onset of creases. We perturb the homogeneous state with a field of small, inhomogeneous strain. We look for the condition under which the homogeneous deformation bifurcates into the inhomogeneous state. This bifurcation corresponds to the onset of wrinkles (Fig. 1c). The inhomogeneous field is governed by linear partial differential equations. Their general solutions under the plane strain conditions can be represented by functions of complex variables (Stroh, 1958). We solve the field using a method of functions of a single complex variable (Suo, 1990). The Stroh formalism has been used to perform linear perturbation analysis by many authors (Suo et al., 1992; Destrade et al., 2009; Weiss et al., 2013).

4.1. Two states with small difference in deformation gradient and pressure

For a body made of an incompressible material, specified by a free energy function $\psi(\mathbf{F})$ and a set of boundary conditions, we ask if the body can be in two distinct states. A standard method to answer this question exists if the difference between the two states is restricted to be small in deformation gradient and pressure. Represent one state by functions $\mathbf{x}^0(\mathbf{X})$ and $\Pi^0(\mathbf{X})$, and the other state by functions $\mathbf{x}(\mathbf{X})$ and $\Pi(\mathbf{X})$. Define the difference of the two fields by the functions

$$\tilde{\mathbf{x}} = \mathbf{x}(\mathbf{X}) - \mathbf{x}^0(\mathbf{X}), \tag{10}$$

$$\tilde{\Pi} = \Pi(\mathbf{X}) - \Pi^0(\mathbf{X}). \tag{11}$$

Similarly write the difference in deformation gradient, stress and traction as $\tilde{\mathbf{F}} = \mathbf{F} - \mathbf{F}^0$, $\tilde{\mathbf{s}} = \mathbf{s} - \mathbf{s}^0$ and $\tilde{\mathbf{T}} = \mathbf{T} - \mathbf{T}^0$.

The two states both satisfy (1)–(5), giving the equations that govern the difference between the two states:

$$\tilde{F}_{iK} = \frac{\partial \tilde{x}_i(\mathbf{X})}{\partial X_K}, \tag{12}$$

$$\frac{\partial \tilde{s}_{iK}(\mathbf{X})}{\partial X_K} = 0, \tag{13}$$

$$\tilde{s}_{iK} N_K = \tilde{T}_i, \tag{14}$$

$$H^0_{iK}\tilde{F}_{iK} = 0, \tag{15}$$

$$\tilde{s}_{iK} = C_{iKjL}(\mathbf{F}^0)\tilde{F}_{jL} - H^0_{iK}\tilde{\Pi}, \tag{16}$$

where $\mathbf{H}^0 = (\mathbf{F}^0)^{-T}$, and the fourth order tensor of tangent moduli is

$$C_{iKjL}(\mathbf{F}^0) = \left[\frac{\partial^2\psi(\mathbf{F})}{\partial F_{iK}\partial F_{jL}}\right]_{\mathbf{F}=\mathbf{F}^0} + \Pi H^0_{iL}H^0_{jK}. \tag{17}$$

In obtaining (15)–(17), we have assumed that the differences in the deformation gradient and in the pressure between the two states are small enough to allow the Taylor expansion around the state $\mathbf{F}^0$ and Π^0. This assumption is valid when the other state represented by $\mathbf{x}(\mathbf{X})$ and $\Pi(\mathbf{X})$ corresponds to wrinkles, but not creases. Given the state represented by $\mathbf{x}^0(\mathbf{X})$ and $\Pi^0(\mathbf{X})$, (12)–(17) define a boundary-value problem that governs the incremental state $\tilde{\mathbf{x}}(\mathbf{X})$ and $\tilde{\Pi}(\mathbf{X})$.

4.2. Represent general solutions using functions of complex variables

We further assume that the state represented by $\mathbf{x}^0(\mathbf{X})$ and $\Pi^0(\mathbf{X})$ is a homogeneous deformation, so that C_{iKjL} is a tensor of the same value for all material particles in the body. A combination of (12), (13) and (16) gives that

$$C_{iKjL}\frac{\partial^2\tilde{x}_j(\mathbf{X})}{\partial X_L\partial X_K} - H^0_{iK}\frac{\partial\tilde{\Pi}(\mathbf{X})}{\partial X_K} = 0. \tag{18}$$

A combination of (12) and (15) gives that

$$H^0_{iK}\frac{\partial\tilde{x}_i(\mathbf{X})}{\partial X_K} = 0. \tag{19}$$

Eqs. (18) and (19) are linear, homogeneous, constant-coefficient, partial differential equations that govern the incremental deformation $\tilde{\mathbf{x}}(\mathbf{X})$ and incremental pressure $\tilde{\Pi}(\mathbf{X})$.

In the stress-free state, the body fills a half space below the plane $X_3 = 0$. Because the incremental field is governed by linear equations, wrinkles of arbitrary shape can be represented by a linear superposition of Fourier components. Each Fourier component corresponds to a field invariant in a direction lying in the (X_1, X_2). We make this direction coincide with the axis X_2. Consequently, the state is represented by functions of two variables, $\tilde{\mathbf{x}}(X_1, X_3)$ and $\tilde{\Pi}(X_1, X_3)$.

We now adopt the method of Stroh (1958) to obtain the general solution to Eqs. (18) and (19). Write both $\tilde{\mathbf{x}}(X_1, X_3)$ and $\tilde{\Pi}(X_1, X_3)$ in terms of a function of a single variable:

$$\tilde{\mathbf{x}}(X_1, X_3) = \mathbf{A}f(z), \tag{20}$$

$$\tilde{\Pi}(X_1, X_3) = Qf'(z) \tag{21}$$

Here $z = X_1 + pX_3$, $f(z)$ is an analytical function, and $f'(z) = df(z)/dz$. The quantities p, Q and A_j are determined as follows.

Substituting (20) and (21) into (18) and (19), we obtain that

$$\left(C_{i1j1} + p\left(C_{i1j3} + C_{i3j1}\right) + p^2C_{i3j3}\right)A_j - \left(H^0_{i1} + pH^0_{i3}\right)Q = 0, \tag{22}$$

$$\left(H^0_{j1} + pH^0_{j3}\right)A_j = 0. \tag{23}$$

These are four linear, homogeneous algebraic equations for A_1, A_2, A_3 and Q, corresponding to an eigenvalue problem. Non-trivial solution exists if and only if

$$\det\mathbf{M} = 0, \tag{24}$$

where

$$M_{ij} = C_{i1j1} + p\left(C_{i1j3} + C_{i3j1}\right) + p^2C_{i3j3},\ M_{i4} = -H^0_{i1} - pH^0_{i3},\ M_{4j} = H^0_{j1} + pH^0_{j3},\ M_{44} = 0, \tag{25}$$

with $i = 1, 2, 3$ and $j = 1, 2, 3$.

Although $\mathbf{M}$ is a four-by-four matrix, we note that $\det\mathbf{M}$ is a sixth-order polynomial of p. A real-valued p would correspond to body waves and spread the incremental field in the entire body. Here we look for surface waves, and assume that all roots of (24) are complex-valued p. Because the coefficients of the sixth-order polynomial are real-valued, the six roots of the polynomials form three complex conjugates. We label the three roots with positive imaginary part by p_α ($\alpha = 1, 2, 3$), and their complex conjugates by $\bar{p}_\alpha$. We label the corresponding quantities solved from the eigenvalue problem by $(A_{1\alpha}, A_{2\alpha}, A_{3\alpha}, Q_\alpha)$ and $\left(\bar{A}_{1\alpha}, \bar{A}_{2\alpha}, \bar{A}_{3\alpha}, \bar{Q}_\alpha\right)$. For each value of α, the quantities $\left(\bar{A}_{1\alpha}, \bar{A}_{2\alpha}, \bar{A}_{3\alpha}, \bar{Q}_\alpha\right)$ can be normalized by an arbitrary complex number.

Let $z_\alpha = X_1 + p_\alpha X_3$, and $f_1(z_1), f_2(z_2), f_3(z_3)$ be three arbitrary analytical functions. The functions $\tilde{\mathbf{x}}(X_1, X_3)$ and $\tilde{\Pi}(X_1, X_3)$ are real-valued. The general solution to (18) and (19) is a linear superposition of the three analytical functions:

$$\tilde{x}_i = \sum_{\alpha=1}^{3} A_{i\alpha} f_\alpha(z_\alpha) + \sum_{\alpha=1}^{3} \bar{A}_{i\alpha} \overline{f_\alpha(z_\alpha)}, \tag{26}$$

$$\tilde{\Pi} = \sum_{\alpha=1}^{3} Q_\alpha f'_\alpha(z_\alpha) + \sum_{\alpha=1}^{3} \bar{Q}_\alpha \overline{f'_\alpha(z_\alpha)}. \tag{27}$$

We use the Greek letter α for the summation over a non-tensor suffix and explicitly indicate the summation.

Substituting (26) and (27) into the equation of state (16), we obtain the incremental nominal stress $\tilde{s}_{iK}$:

$$\tilde{s}_{i3} = \sum_{\alpha=1}^{3} L_{i\alpha} f'_\alpha(z_\alpha) + \sum_{\alpha=1}^{3} \bar{L}_{i\alpha} \overline{f'_\alpha(z_\alpha)}, \tag{28}$$

$$\tilde{s}_{i1} = -\sum_{\alpha=1}^{3} L_{i\alpha} p_\alpha f'_\alpha(z_\alpha) - \sum_{\alpha=1}^{3} \bar{L}_{i\alpha} \bar{p}_\alpha \overline{f'_\alpha(z_\alpha)}, \tag{29}$$

where

$$L_{i\alpha} = \left(C_{i3j1} + p_\alpha C_{i3j3}\right) A_{j\alpha} - H_{i3} Q_\alpha. \tag{30}$$

For the incompressible Gent material, the tangent moduli C_{iKjL} and the components of the matrices $A_{i\alpha}$, Q_α and $L_{i\alpha}$ are given in the Appendix A.

4.3. Critical condition for the onset of wrinkles

The Stroh representation involves three complex variables. We now derive the critical condition for the onset of wrinkles using the method of a single complex variable (Suo, 1990). Let z be a complex variable of the form $z = X_1 + qX_3$, with q being an arbitrary complex number with a positive imaginary part. Observe that at the surface of the body, $X_3 = 0$, the complex variable z coincides with z_1, z_2 and z_3 defined above. Write

$$\mathbf{f}(z) = \left[f_1(z), f_2(z), f_3(z)\right]^T. \tag{31}$$

Once we obtain $\mathbf{f}(z)$ for any z, we can replace z with z_1, z_2 and z_3, and use $f_1(z_1)$, $f_2(z_2)$ and $f_3(z_3)$ to describe the wrinkled state.

The surface of the body ($X_3 = 0$) is traction-free, so that (28) reduces to

$$\mathbf{L}\mathbf{f}'(X_1) + \bar{\mathbf{L}}\bar{\mathbf{f}}'(X_1) = 0. \tag{32}$$

This equation sets the boundary condition for the function $\mathbf{f}(z)$. The boundary-value problem is solved as follows. Assume that the material occupies the lower half plane ($X_3 \le 0$). Because no singularity is present in the material, $\mathbf{L}\mathbf{f}'(z)$ is a function analytic in the lower half plane. Consequently, $\bar{\mathbf{L}}\bar{\mathbf{f}}'(z)$ is a function analytic in the upper half plane. By the theorem of analytic continuation, the boundary condition (32) requires that both functions be analytic in the entire plane (Carrier et al., 1983). The wrinkles are disturbance localized on the surface of the gel, so that the analytic functions vanish as $|z| \to \infty$. The only function analytic in the entire plane and vanishing as $|z| \to \infty$ is the function being zero everywhere. Consequently, the solution to the boundary-value problem (32) is

$$\mathbf{L}\mathbf{f}'(z) = 0. \tag{33}$$

Eq. (33) is an eigenvalue problem. A nontrivial solution of $\mathbf{f}'(z)$ exists if and only if

$$\det\mathbf{L} = 0. \tag{34}$$

For the in-plane deformation of a Gent material, a combination of (34) and (A.11) gives the critical condition for the onset of wrinkles. The determinant of $\mathbf{L}$ is a purely imaginary number. Fig. 6 plots $\det\mathbf{L}\left(J_{lim} - J_1\right)^2/\mu^2 {J_{lim}}^2 i$ as a function of the applied strain. As J_{lim} increases, the curves approach the behavior of the limiting case for the neo-Hookean materials, $J_{\lim} \to \infty$. When $J_{\lim} \to \infty$, the solution $\varepsilon = 0.456$ recovers the Biot condition for the onset of wrinkles in a neo-Hookean material. When $J_{\lim} > 8.169$, there are two admissible solutions. When $J_{\lim} = 8.169$, Eq. (34) has a unique solution $\varepsilon = 0.580$. When $J_{\lim} < 8.169$, Eq. (34) has no solution, i.e. no wrinkles are predicted by the linear perturbation method.

The critical conditions for the formation of wrinkles obtained by the linear perturbation analysis are compared with those of creases (Fig. 5). As J_{lim} decreases, the branch of smaller strains increases, but the branch of larger strains decreases. Observe that creases always form at a smaller strain than wrinkles. Thus, neither branch of wrinkles can be realized. Creases, rather than wrinkles, should be observed in the Gent materials.

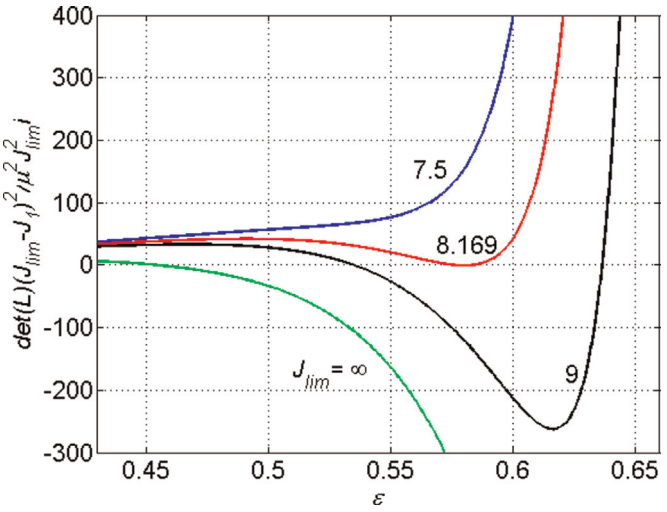

Fig. 6. The critical strains for wrinkles are determined by $\det\mathbf{L} = 0$. Plotted here are $det\mathbf{L}\left(J_{lim} - J_1\right)^2/\mu^2 J_{lim}{}^2 i$ as a function of the applied strain ε for different values of J_{lim}. When $J_{\lim} \to \infty$, the solution $\varepsilon = 0.456$ recovers the Biot condition for the onset of wrinkles in a neo-Hookean material. When $J_{\lim} > 8.169$, $\det\mathbf{L}$ becomes zero at two values of the applied strain. When $J_{\lim} = 8.169$, $\det\mathbf{L} = 0$ has a single solution $\varepsilon = 0.580$. When $J_{\lim} < 8.169$, $\det(\mathbf{L})$ cannot reach zero at any applied strain.

Once the critical strain is determined by (34), the eigenvector is

$$\begin{bmatrix} e_1 \\ e_3 \end{bmatrix} = \begin{bmatrix} 1 \\ -L_{11}/L_{13} \end{bmatrix}. \tag{35}$$

Consequently, the field of the wrinkled state is determined by $f_1'(z_1) = w(z_1)$ and $f_3'(z_3) = -(L_{11}/L_{13})w(z_3)$, where $w(z)$ is an arbitrary scalar-valued function.

5. Conclusions and discussions

In this paper, we study the initiation and development of creases in strain-stiffening materials. As a result, strain-stiffening effect raises the critical strain for crease initiation and smoothens creases when the compressive strain is large enough. When the strain-stiffening effect is strong enough, creases can be completely suppressed. As a comparison, we also study the initiation of wrinkles in strain-stiffening materials by the linear perturbation method under Stroh formalism. The classical Stroh formalism is extended for incompressible materials. Our calculations show that creases always form at a lower strain than wrinkles, and should be observed.

The stretchability of soft tissues varies with age, pathology, humidity, as well as the type of tissues. Tendons and ligaments can be uniaxially stretched to a strain of around 15% (Holzapfel, 2001), cartilage 120% (Holzapfel, 2001), skins 110% (Dunn et al., 1985), and aorta 100% (Holzapfel, 2001). These values correspond to $J_{lim} = 0.06, 2.75, 2.36$ and 2.00, respectively. These small values of J_{lim} suggests that strain-stiffening effect can play a significant role to suppress the formation of creasing in these soft tissues.

For polymers, the limiting stretch can be estimated as $\sqrt{n}$, with n being the number of monomers between two cross-linkers. The value of n can be as small as several or as large as thousands, and $J_{\lim}$ can be correspondingly tuned by changing the crosslink density. The value of $J_{\lim}$ can also be tuned by mixing polymers of different kinds. It is hoped that our theoretical prediction of the smoothening and suppressing of creases can soon be demonstrated experimentally.

Acknowledgments

This work was supported by the NSF MRSEC (DMR-0820484). We thank Philipp Rothemund and Katia Bertoldi at Harvard University for the discussion on the implementation of Gent user subroutine in ABAQUS.

Appendix A. Tangent moduli C and matrices A, Q and L of the Gent materials

When the material is specified as an incompressible Gent material with free energy as shown in (6), according to (17), we obtain the tensor of tangent moduli:

$$C_{iKjL} = \frac{\mu}{1 - J_1/J_{lim}}\delta_{ij}\delta_{KL} + \frac{2\mu J_{\lim}^{-1}}{\left(1 - J_1/J_{lim}\right)^2}F^0_{iK}F^0_{jL} + \Pi H^0_{iL}H^0_{jK}. \tag{A1}$$

The field of finite deformation before perturbation is under a homogeneous plane strain condition, and the principal stretches are in the directions coinciding with X_1, X_2 and X_3. Consequently, $\mathbf{F}^0 = diag\left(\lambda, 1, \lambda^{-1}\right)$, $\mathbf{H}^0 = diag\left(\lambda^{-1}, 1, \lambda\right)$. The hydrostatic pressure Π^0 is determined by the boundary condition $s_{33} = 0$, and according to (7), we get $\Pi^0 = \mu\lambda^{-2}/\left(1 - J_1/J_{lim}\right)$. The tangent moduli reduce to the following nonzero elements:

$$C_{1111} = \frac{\mu(1+\lambda^{-4})}{1 - J_1/J_{lim}} + \frac{2\mu\lambda^2 J_{\lim}^{-1}}{\left(1 - J_1/J_{lim}\right)^2},\ C_{2222} = \frac{\mu(1+\lambda^{-2})}{1 - J_1/J_{lim}} + \frac{2\mu J_{\lim}^{-1}}{\left(1 - J_1/J_{lim}\right)^2},\ C_{3333} = \frac{2\mu}{1 - J_1/J_{lim}} + \frac{2\mu\lambda^{-2}J_{\lim}^{-1}}{\left(1 - J_1/J_{lim}\right)^2} \tag{A2}$$

$$C_{1212} = C_{2121} = C_{1313} = C_{3131} = C_{3232} = C_{2323} = \frac{\mu}{1 - J_1/J_{lim}}, \tag{A3}$$

$$C_{1122} = C_{2211} = \frac{2\mu\lambda J_{\lim}^{-1}}{\left(1 - J_1/J_{lim}\right)^2},\ C_{1133} = C_{3311} = \frac{2\mu J_{\lim}^{-1}}{\left(1 - J_1/J_{lim}\right)^2},\ C_{2233} = C_{3322} = \frac{2\mu\lambda^{-1}J_{\lim}^{-1}}{\left(1 - J_1/J_{lim}\right)^2}, \tag{A4}$$

$$C_{2112} = C_{1221} = \frac{\mu\lambda^{-3}}{1 - J_1/J_{lim}},\ C_{3113} = C_{1331} = \frac{\mu\lambda^{-2}}{1 - J_1/J_{lim}},\ C_{3223} = C_{2332} = \frac{\mu\lambda^{-1}}{1 - J_1/J_{lim}}. \tag{A5}$$

Next we substitute (A2)–(A5) to the Stroh formalism. The complex numbers p_1 and p_3 are determined by (24), which is specialized to

$$\lambda^2 p^4 + g(\lambda)p^2 + \lambda^{-2} = 0, \tag{A6}$$

where

$$g(\lambda) = \frac{2}{J_{\lim} - J_1}(\lambda^4 + \lambda^{-4} - 2) + \lambda^2 + \lambda^{-2}. \tag{A7}$$

The two roots with positive imaginary part of the above equation are

$$p_1 = i\sqrt{\frac{g(\lambda) + \sqrt{g(\lambda)^2 - 4}}{2\lambda^2}},\ p_3 = i\sqrt{\frac{g(\lambda) - \sqrt{g(\lambda)^2 - 4}}{2\lambda^2}}. \tag{A8}$$

The components of the matrices $A_{i\alpha}$, Q_α and $L_{i\alpha}$ for the in-plane deformation are

$$A_{11} = p_1,\ A_{13} = p_3,\ A_{31} = -\lambda^{-2},\ A_{33} = -\lambda^{-2}; \tag{A9}$$

$$Q_1 = \frac{\mu\lambda p_1}{1 - J_1/J_{lim}}\left[\left(1 + {p_1}^2\right) + \frac{2}{J_{\lim} - J_1}(\lambda^2 - \lambda^{-2})\right],\ Q_3 = \frac{\mu\lambda p_3}{1 - J_1/J_{lim}}\left[\left(1 + {p_3}^2\right) + \frac{2}{J_{\lim} - J_1}(\lambda^2 - \lambda^{-2})\right]; \tag{A10}$$

$$\begin{aligned}
L_{11} &= \frac{\mu}{1 - J_1/J_{lim}}\left({p_1}^2 - \lambda^{-4}\right),\\
L_{13} &= \frac{\mu}{1 - J_1/J_{lim}}\left({p_3}^2 - \lambda^{-4}\right),\\
L_{31} &= -\frac{\mu p_1}{1 - J_1/J_{lim}}\left(g(\lambda) + \lambda^{-2} + \lambda^2 {p_1}^2\right),\\
L_{33} &= -\frac{\mu p_3}{1 - J_1/J_{lim}}\left(g(\lambda) + \lambda^{-2} + \lambda^2 {p_3}^2\right).
\end{aligned} \tag{A11}$$

Appendix B. Implementation of the Gent material in ABAQUS

We implement the Gent model in the finite element software ABAQUS by writing a user-defined material subroutine, UMAT. We use a compressible form of the Gent free energy density (Wang et al., 2013)

$$\psi = -\frac{\mu}{2}J_{lim}\log\left(1-\frac{J_1}{J_{lim}}\right)-\mu\log(J)+\left(\frac{K}{2}-\frac{\mu}{J_{lim}}\right)(J-1)^2, \tag{B1}$$

where $J=\det(\mathbf{F})$ and the parameter K is the bulk modulus. The last two terms in (B1) is the energy density related to a volume change, and they are non-zero when $J\neq 1$. The incompressible Gent material (6) can be recovered in the limit, $K/\mu\to\infty$.

In the user subroutine UMAT, the Cauchy stress tensor $\boldsymbol{\sigma}$, defined as $\boldsymbol{\sigma}=(1/J)(\partial\psi/\partial\mathbf{F})\mathbf{F}^T$, is implemented as

$$\sigma_{ij}=\frac{\mu J^{-1}}{1-J_1/J_{lim}}F_{iK}F_{jK}+\left(2\left(\frac{K}{2}-\frac{\mu}{J_{lim}}\right)(J-1)-\frac{\mu}{J}\right)\delta_{ij}. \tag{B2}$$

The fourth order Jacobian tensor $\mathbf{D}$ is defined as

$$\delta\left(J\sigma_{ij}\right)=JD_{ijmn}(\delta F_{mK}H_{nK}+\delta F_{nK}H_{mK})/2, \tag{B3}$$

which can be calculated as (Wilson, 2005)

$$D_{ijmn}=\left(\sigma_{ij}H_{nK}+\frac{\delta\sigma_{ij}}{\delta F_{nK}}\right)F_{mK}. \tag{B4}$$

For a Gent material, it can be derived that

$$\frac{\delta\sigma_{ij}}{\delta F_{nK}}=\frac{\mu J^{-1}}{1-J_1/J_{lim}}\left(\delta_{in}F_{jK}+\delta_{jn}F_{iK}\right)+\frac{2\mu J_{\lim}^{-1}J^{-1}}{\left(1-J_1/J_{lim}\right)^2}F_{iL}F_{jL}F_{nK}\qquad+\left(\left(J\left(K-\frac{2\mu}{J_{lim}}\right)+\frac{\mu}{J}\right)\delta_{ij}-\frac{\mu J^{-1}}{1-J_1/J_{lim}}F_{iL}F_{jL}\right)H_{nK}. \tag{B5}$$

Substituting (B2) and (B5) into (B4), we can calculate the Jacobian tensor.

In the ABAQUS subroutine UMAT, we need to implement the Cauchy stress tensor (B2), the Jacobian tensor (B4), and the free energy density (B1). The UMAT checks how far the state is from the limiting stretch for every material particle in every increment to ensure that the state stays within the limit $J_1=J_{lim}$. We implement this requirement in the UMAT as follows. The calculation is conducted incrementally. After the UMAT finishes the calculation at a given increment, if $J_{lim}-J_1<1e-3$, the UMAT abandons the original increment, and attempts the calculation again with an increment half of the original one. Then the UMAT checks the criterion $J_{lim}-J_1<1e-3$ again. The UMAT attempts to satisfy the criterion $J_{lim}-J_1<1e-3$ for a maximal times, say 5 times; if not, the UMAT aborts the simulation.

Appendix C. Supplementary information

Supplementary data associated with this article can be found in the online version at http://dx.doi.org/10.1016/j.jmps.2014.10.004.

References

Arifuzzaman, M., Wu, Z.L., Kurokawa, T., Kakugo, A., Gong, J.P., 2012. Swelling-induced long-range ordered structure formation in polyelectrolyte hydrogel. Soft Matter 8, 8060–8066.
Barros, W., de Azevedo, E.N., Engelsberg, M., 2012. Surface pattern formation in a swelling gel. Soft Matter 8, 8511–8516.
Bayly, P.V., Taber, L.A., Kroenke, C.D., 2014. Mechanical forces in cerebral cortical folding: a review of measurements and models. J. Mech. Behav. Biomed. 29, 568–581.
Biot, M.A., 1963. Surface instability of rubber in compression. Appl. Sci. Res. 12, 168–182.
Bowden, N., Brittain, S., Evans, A.G., Hutchinson, J.W., Whitesides, G.M., 1998. Spontaneous formation of ordered structures in thin films of metals supported on an elastomeric polymer. Nature 393, 146–149.
Cai, S.Q., Bertoldi, K., Wang, H.M., Suo, Z.G., 2010. Osmotic collapse of a void in an elastomer: breathing, buckling and creasing. Soft Matter 6, 5770–5777.
Cai, S.Q., Chen, D.Y., Suo, Z.G., Hayward, R.C., 2012. Creasing instability of elastomer films. Soft Matter 8, 1301–1304.
Cao, Y.P., Hutchinson, J.W., 2012. From wrinkles to creases in elastomers: the instability and imperfection-sensitivity of wrinkling. Proc. R. Soc. London A Math. 468, 94–115.
Carrier, G.F., Krook, M., Pearson, C.E., 1983. Functions of a Complex Variable: Theory and Technique. Hod Books, Ithaca.
Chan, E.P., Karp, J.M., Langer, R.S., 2011. A self-pinning adhesive based on responsive surface wrinkles. J. Polym. Sci. Polym. Phys. 49, 40–44.
Chen, D.Y., Cai, S.Q., Suo, Z.G., Hayward, R.C., 2012. Surface energy as a barrier to creasing of elastomer films: an elastic analogy to classical nucleation. Phys. Rev. Lett. 109, 038001.
Chen, D., Jin, L., Suo, Z., Hayward, R.C., 2014. Controlled formation and disappearance of creases. Mater. Horiz. 1, 207–213.

Dervaux, J., Ben Amar, M., 2012. Mechanical instabilities of gels. Annu. Rev. Condens. Matter Phys. 3, 311–332.
Dervaux, J., Couder, Y., Guedeau-Boudeville, M.A., Ben Amar, M., 2011. Shape transition in artificial tumors: from smooth buckles to singular creases. Phys. Rev. Lett. 107, 018103.
Destrade, M., Annaidh, A.N., Coman, C.D., 2009. Bending instabilities of soft biological tissues. Int. J. Solids Struct. 46, 4322–4330.
Diab, M.Z., Zhang, T., Zhao, R.K., Gao, H.J., Kim, K.S., 2013. Ruga mechanics of creasing: from instantaneous to setback creases. Proc. R. Soc. London A Math. 469, 20120753.
Dunn, M.G., Silver, F.H., Swann, D.A., 1985. Mechanical analysis of hypertrophic scar tissue: structural basis for apparent increased rigidity. J. Invest. Dermatol. 84, 9–13.
Fung, Y.C., 1993. Biomechanics: Material Properties of Living Tissues. Springer, New York.
Gabriel, P., Fukahori, Y., Thomas, A.G., Busfield, J.J.C., 2010. FEA modeling of Schallamach waves. Rubber Chem. Technol. 83, 358–367.
Gent, A.N., 1996. A new constitutive relation for rubber. Rubber Chem. Technol. 69, 59–61.
Gent, A.N., Cho, I.S., 1999. Surface instabilities in compressed or bent rubber blocks. Rubber Chem. Technol. 72, 253–262.
Ghatak, A., Das, A.L., 2007. Kink instability of a highly deformable elastic cylinder. Phys. Rev. Lett. 99, 076101.
Guvendiren, M., Burdick, J.A., Yang, S., 2010. Solvent induced transition from wrinkles to creases in thin film gels with depth-wise crosslinking gradients. Soft Matter 6, 5795–5801.
Hohlfeld, E., 2008. Creasing, Post-bifurcations and the Spontaneous Breakdown of Scale Invariance (Ph.D. thesis). Harvard University, Cambridge, MA.
Hohlfeld, E., 2013. Coexistence of scale-invariant states in incompressible elastomers. Phys. Rev. Lett. 111, 185701.
Hohlfeld, E., Mahadevan, L., 2011. Unfolding the Sulcus. Phys. Rev. Lett. 106, 105702.
Hohlfeld, E., Mahadevan, L., 2012. Scale and nature of sulcification patterns. Phys. Rev. Lett. 109, 025701.
Holzapfel, G.A., 2000. In: Nonlinear Solid Mechanics: A Continuum Approach for EngineeringJohn Wiley & Sons, Chichester.
Holzapfel, G.A., 2001. Biomechanics of soft tissue. In: Lemaitre, J. (Ed.), The Handbook of Materials Behavior Models, Volume III, Multiphysics Behaviors. Academic Press, Boston, pp. 1049–1063.
Hong, W., Zhao, X.H., Suo, Z.G., 2009. Formation of creases on the surfaces of elastomers and gels. Appl. Phys. Lett. 95, 111901.
Hong, W., Gao, F., 2013. Crease instability on the surface of a solid. In: Chen, X. (Ed.), Mechanical Self-assembly. Springer, New York, pp. 111–130.
Hutchinson, J.W., 2013. The role of nonlinear substrate elasticity in the wrinkling of thin films. Philos. Trans. R. Soc. A 371, 20120422.
Jin, L.H., Cai, S.Q., Suo, Z.G., 2011. Creases in soft tissues generated by growth. Europhys. Lett. 95, 64002.
Jin, L.H., Chen, D.Y., Hayward, R.C., Suo, Z.G., 2014. Creases on the interface between two soft materials. Soft Matter 10, 303–311.
Kim, J., Yoon, J., Hayward, R.C., 2010. Dynamic display of biomolecular patterns through an elastic creasing instability of stimuli-responsive hydrogels. Nat. Mater. 9, 159–164.
Mora, S., Abkarian, M., Tabuteau, H., Pomeau, Y., 2011. Surface instability of soft solids under strain. Soft Matter 7, 10612–10619.
Ortiz, O., Vidyasagar, A., Wang, J., Toomey, R., 2010. Surface instabilities in ultrathin, cross-linked poly(N-isopropylacrylamide) coatings. Langmuir 26, 17489–17494.
Pandey, A., Holmes, D.P., 2013. Swelling-induced deformations: a materials-defined transition from macroscale to microscale deformations. Soft Matter 9, 5524–5528.
Park, H.S., Wang, Q.M., Zhao, X.H., Klein, P.A., 2013. Electromechanical instability on dielectric polymer surface: modeling and experiment. Comput. Method Appl. Mech. Eng. 260, 40–49.
Pocivavsek, L., Dellsy, R., Kern, A., Johnson, S., Lin, B.H., Lee, K.Y.C., Cerda, E., 2008. Stress and fold localization in thin elastic membranes. Science 320, 912–916.
Saha, K., Kim, J., Irwin, E., Yoon, J., Momin, F., Trujillo, V., Schaffer, D.V., Healy, K.E., Hayward, R.C., 2010. Surface creasing instability of soft polyacrylamide cell culture substrates. Biophys. J. 99, 94–96.
Shivapooja, P., Wang, Q., Orihuela, B., Rittschof, D., Lopez, G.P., Zhao, X., 2013. Bioinspired surfaces with dynamic topography for active control of biofouling. Adv. Mater. 25, 1430–1434.
Stroh, A.N., 1958. Dislocations and cracks in anisotropic elasticity. Philos. Mag. 3, 625–646.
Suo, Z., 1990. Singularities interfaces and cracks in dissimilar anistropic media. Proc. R. Soc. London A Math. 427 (331–358).
Suo, Z., Ortiz, M., Needleman, A., 1992. Stability of solids with interfaces. J. Mech. Phys. Solids 40, 613–640.
Tallinen, T., Biggins, J.S., Mahadevan, L., 2013. Surface sulci in squeezed soft solids. Phys. Rev. Lett. 110, 024302.
Tanaka, T., 1986. Kinetics of phase transition in polymer gels. Physica A 140, 261–268.
Tanaka, T., Sun, S.T., Hirokawa, Y., Katayama, S., Kucera, J., Hirose, Y., Amiya, T., 1987. Mechanical instability of gels at the phase transition. Nature 325, 796–798.
Treloar, L.R.G., 1975. In: The Physics of Rubber Elasticitythird ed. Clarendon Press, Oxford.
Trujillo, V., Kim, J., Hayward, R.C., 2008. Creasing instability of surface-attached hydrogels. Soft Matter 4, 564–569.
Wang, P., Shim, J.M., Bertoldi, K., 2013. Effects of geometric and material nonlinearities on tunable band gaps and low-frequency directionality of phononic crystals. Phys. Rev. B 88, 014304.
Wang, Q.M., Niu, X.F., Pei, Q.B., Dickey, M.D., Zhao, X.H., 2012. Electromechanical instabilities of thermoplastics: theory and in situ observation. Appl. Phys. Lett. 101, 141911.
Wang, Q.M., Zhang, L., Zhao, X.H., 2011. Creasing to cratering instability in polymers under ultrahigh electric fields. Phys. Rev. Lett. 106, 118301.
Wang, Q.M., Zhao, X.H., 2013a. Creasing-wrinkling transition in elastomer films under electric fields. Phys. Rev. E 88, 042403.
Wang, Q.M., Zhao, X.H., 2013b. Phase diagrams of instabilities in compressed film-substrate systems. J. Appl. Mech. Trans. ASME 81, 051004.
Weiss, F., Cai, S., Hu, Y., Kang, M.K., Huang, R., Suo, Z., 2013. Creases and wrinkles on the surface of a swollen gel. J. Appl. Phys. 114, 073507.
Wilson, W., 2005. An Explanation for the Onset of Mechanically Induced Cartilage Damage (Ph.D. thesis). Technische Universiteit Eindhoven, Eindhoven.
Wong, W.H., Guo, T.F., Zhang, Y.W., Cheng, L., 2010. Surface instability maps for soft materials. Soft Matter 6, 5743–5750.
Wu, Z.G., Bouklas, N., Huang, R., 2013. Swell-induced surface instability of hydrogel layers with material properties varying in thickness direction. Int. J. Solids Struct. 50, 578–587.
Xu, B., Hayward, R.C., 2013. Low-voltage switching of crease patterns on hydrogel surfaces. Adv. Mater. 25, 5555–5559.
Yang, W., Fung, T.C., Chian, K.S., Chong, C.K., 2007. Instability of the two-layered thick-walled esophageal model under the external pressure and circular outer boundary condition. J. Biomech. 40, 481–490.
Yoon, J., Bian, P., Kim, J., McCarthy, T.J., Hayward, R.C., 2012. Local switching of chemical patterns through light-triggered unfolding of creased hydrogel surfaces. Angew. Chem. Int. Ed. 51, 7146–7149.
Yoon, J., Kim, J., Hayward, R.C., 2010. Nucleation, growth, and hysteresis of surface creases on swelled polymer gels. Soft Matter 6, 5807–5816.
Zalachas, N., Cai, S.Q., Suo, Z.G., Lapusta, Y., 2013. Crease in a ring of a pH-sensitive hydrogel swelling under constraint. Int. J. Solids Struct. 50, 920–927.
Zang, J.F., Zhao, X.H., Cao, Y.P., Hutchinson, J.W., 2012. Localized ridge wrinkling of stiff films on compliant substrates. J. Mech. Phys. Solids 60, 1265–1279.